

HMapNet: An Online HD Map Construction and Evaluation Framework

Qi Li*
Tsinghua University
liqil17thu@gmail.com

Yue Wang*
MIT
yuewangx@mit.edu

Yilun Wang
Li Auto
yilunw@cs.stanford.edu

Hang Zhao
Tsinghua University
hangzhao@mail.tsinghua.edu.cn

Abstract: High-definition map (HD map) construction is a crucial problem for autonomous driving. This problem typically involves collecting high-quality point clouds, fusing multiple point clouds of the same scene, annotating map elements, and updating maps constantly. This pipeline, however, requires a vast amount of human efforts and resources which limits its scalability. Additionally, traditional HD maps are coupled with centimeter-level accurate localization which is unreliable in many scenarios [1]. In this paper, we argue that online map learning, which dynamically constructs the HD maps based on local sensor observations, is a more scalable way to provide semantic and geometry priors to self-driving vehicles than traditional pre-annotated HD maps. Meanwhile, we introduce an online map learning method, titled HMapNet. It encodes image features from surrounding cameras and/or point clouds from LiDAR, and predicts vectorized map elements in the bird’s-eye view. We benchmark HMapNet on the nuScenes dataset and show that in all settings, it performs better than baseline methods. Of note, our fusion-based HMapNet outperforms existing methods by more than 50% in all metrics. To accelerate future research, we develop customized metrics to evaluate map learning performance, including both semantic-level and instance-level ones. By introducing this method and metrics, we invite the community to study this novel map learning problem. We will release our code and evaluation kit to facilitate future development.

Keywords: Autonomous Driving, Computer Vision, High-definition Maps

1 Introduction

High-definition maps (HD maps) are an essential module for autonomous driving. An HD Map contains centimeter-level geometry and semantic information of road elements such as lane markings, dividers, road boundaries, and the roads’ topology that are annotated by human annotators or semi-automatic algorithms. It enables autonomous vehicles to localize themselves precisely [2, 3], predict other objects’ motions [4, 5], and plan beyond sensor visibility [6, 7].

However, classical pipelines of annotating and maintaining HD maps pose many challenges. First, point clouds are collected by a mobile mapping system (MMS) equipped with LiDARs, GPS, IMUs, and wheel odometers. Precise calibrations between these sensors and constant maintenance are needed to ensure the accuracy of HD maps, making MMS hard to scale up. Second, multiple point clouds of the same scene are fused by simultaneous localization and mapping (SLAM) algorithms [8, 9, 10], to ensure a high-quality, dense point cloud representation of the environment. Minor errors in SLAM can lead to large misalignments in the final point clouds. Third, the fused point clouds are annotated manually or semi-automatically with the roads’ geometry, semantic labels (*e.g.* lanes and road boundaries), and the topology of the driving areas. Annotating HD maps asks for a great deal

*Equal contribution.

†project page: <https://tsinghua-mars-lab.github.io/HMapNet/>

of human labor and resources [11]. Moreover, road conditions are ever-changing, to enable long-term use, HD maps demand constant updates and maintenance. This gives rise to non-decreasing amortized costs. Finally, centimeter-level localization algorithms have to be developed to localize autonomous vehicles within HD maps. Reliable and all-weather localization algorithms are still open problems [12, 1], which further limit HD maps’ scalability.

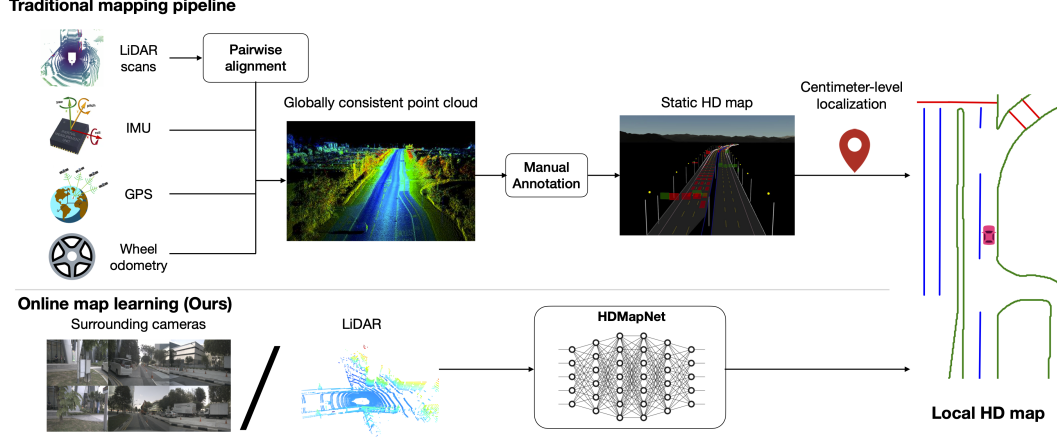


Figure 1: Comparisons of a traditional mapping pipeline and our online map learning pipeline.

As an alternative approach to pre-annotate global HD maps, we introduce a novel online map learning framework that makes use of onboard sensors and computation to estimate local maps. In contrast to past works, our framework does not maintain or update HD maps, removing humans’ necessity in the loop, which makes it simpler and more scalable.

Meanwhile, we propose a concrete map learning method called HDMaPNet, which produces vectorized map elements from images of the surrounding cameras and/or from point clouds like LiDARs. In HDMaPNet, we study how to effectively transform perspective image features to bird’s-eye view features when depth is missing. We put forward a novel view transformer that consists of both neural feature transformation and geometric projection. Moreover, we investigate whether point clouds and camera images complement each other in this task. We find different map elements are not equally recognizable in a single modality. To take the best from both worlds, our best model combines point cloud representations with image representations. This model outperforms its single-modal counterparts by a significant margin in all categories.

Finally, we propose comprehensive ways to evaluate the performance of map construction. These metrics include both semantic level and instance level evaluations as map elements are typically represented as instances in HD maps.

To summarize, our contributions include the following:

- We propose a new framework, online HD map learning, that is a lower-cost and more scalable approach than classical HD mapping and localization pipelines.
- We put forward HDMaPNet that predicts bird’s-eye view HD maps directly from the surround-view cameras and/or LiDAR observations. Our model improves over existing methods by 12.1 IoU on semantic segmentation and 13.1 mAP on instance detection.
- We come up with a novel feature projection module from perspective view to bird’s-eye view. This module models 3D environments implicitly and considers the camera extrinsic explicitly.
- We develop comprehensive evaluation protocols and metrics for the online HD map learning task.

2 Related Work

Classical mapping pipeline. Most existing HD Maps are annotated either manually or semi-automatically on LiDAR point clouds of the environment, merged from LiDAR scans collected from survey vehicles with high-end GPS and IMU. SLAM algorithms are the most commonly used algorithms to fuse LiDAR scans into a highly accurate and consistent point cloud. First, pairwise

alignment algorithm like ICP [13], NDT [14] and their variants [15] are employed to match LiDAR data at two nearby timestamps using semantic [16] or geometry information [17]. Second, estimating accurate poses of ego vehicle is formulated as a non-linear least-square problem [18] or a factor graph [19] which is critical to build a globally consistent map. Yang *et al.* [10] presented a method for reconstructing HD maps at city scale based on the pose graph optimization under the constraint of pairwise alignment factor. To reduce the cost of manual annotation of HD map, Jian *et al.* [11] proposed several machine learning techniques to extract static elements from fused LiDAR point cloud and cameras. However, it is still laborious and costly to maintain an HD map since it requires high precision and timely update. In this paper, we argue that our proposed online map construction task is more scalable and practical than the classical mapping pipeline.

Perspective view lane detection. The traditional perspective-view-based lane detection pipeline involves local image feature extraction (*e.g.* color, directional filters [20, 21, 22]), line fitting (*e.g.* Hough transform [23]), image-to-world projection, *etc.* With the advances of deep learning based image segmentation and detection techniques [24, 25, 26, 27], researchers have explored more data-driven approaches. Deep models were developed for road segmentation [28, 29], lane detection [30, 31], drivable area analysis [32], *etc.* More recently, models were built to give 3D outputs rather than 2D. Bai *et al.* [33] incorporated LiDAR signals so that image pixels can be projected onto the ground. Garnett *et al.* [34] and Guo *et al.* [35] used synthetic lane datasets to perform supervised training on the prediction of camera height and pitch, so that the output lanes sit in a 3D ground plane. Beyond detecting lanes, our work aims to output a consistent HD map around the vehicle from surround cameras or LiDARs.

Cross-view learning. Recently, some efforts have been made to study cross-view learning to facilitate robots’ surrounding sensing capability. These works share a similar framework that encodes image features in perspective view and transforms features into bird’s-eye view to be decoded into various sensing targets. Pan [36] used multilayer perceptron (MLP) to learn the relationship between any two pixel positions in flattened perspective-view feature maps and flattened bird’s-eye view feature maps. Roddick and Cipolla [37] collapsed image feature map into a bottleneck feature by only preserving horizontal dimension. 1D convolution is then used along the horizontal axis to reshape the feature map, and camera intrinsic parameters were used to resample into bird’s-eye view. Philion and Fidler [38] predicted the depth of monocular cameras and project image features into bird’s-eye view using soft attention. Our work focuses on the crucial task of online map construction that we use cross-view sensing methods to generate maps in an end-to-end way. We show that our model outperforms prior projection methods in Section 4. Moreover, our model can be easily fused with LiDAR input to improve its accuracy further.

3 Online HD Map Learning

We propose online HD map learning, a novel framework that produces HD maps online. It takes sensor inputs like camera images and LiDAR point clouds, and outputs vectorized map elements, such as lane dividers, lane boundaries and pedestrian crossings. We use \mathcal{I} and \mathcal{P} to denote the images and point clouds, respectively. Optionally, the framework can be extended to include other sensor signals like radars. We define \mathcal{M} as the map elements to predict.

In Section 3.1, we will discuss our proposed method for online HD map learning; in Section 3.2, we will develop metrics to evaluate map learning methods.

3.1 HMapNet

Classic algorithms typically deploy complicated pipelines to merge data from multiple sensors and require significant human efforts in the loop. Our HD map learning method, named HMapNet, instead predicts map elements \mathcal{M} from single frame \mathcal{I} and \mathcal{P} with neural networks directly. An overview of the model is shown in Figure 2, four neural networks parameterize our model: a perspective view image encoder $\phi_{\mathcal{I}}$ and a neural view transformer $\phi_{\mathcal{V}}$ in the image branch, a pillar-based point cloud encoder $\phi_{\mathcal{P}}$, and a map element decoder $\phi_{\mathcal{M}}$. We denote our HMapNet family as HMapNet(Surr), HMapNet(LiDAR), HMapNet(Fusion) if the model takes only surrounding images, only LiDAR, or both of them as input.

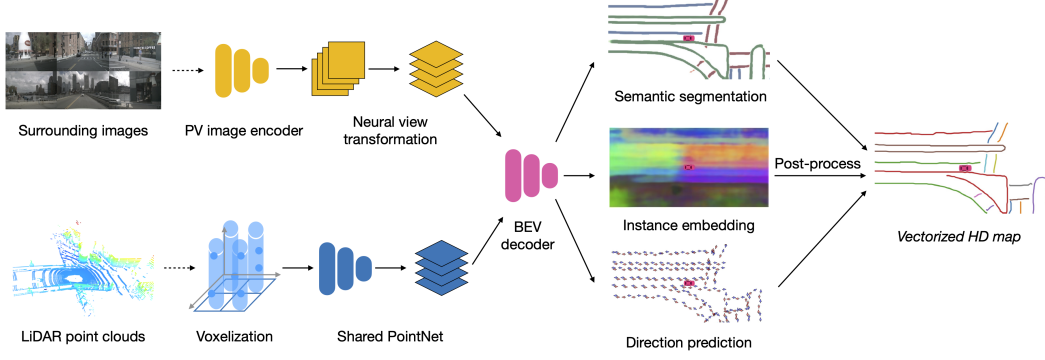


Figure 2: Model overview. Our model works with either or both of images and point clouds, outputs semantic segmentation, instance embedding and directions, and finally produces a vectorized HD map. Top left: image branch. Bottom left: point cloud branch. Right: vectorized HD Map.

3.1.1 Image encoder

Perspective view image encoder. Our image branch takes perspective view inputs from N_m surrounding cameras, covering the panorama of the scene. Each image \mathcal{I}_i is embedded by a shared neural network $\phi_{\mathcal{I}}$ to get perspective view feature map $\mathcal{F}_{\mathcal{I}_i}^{\text{pv}} \subseteq \mathbb{R}^{H_{\text{pv}} \times W_{\text{pv}} \times K}$ where H_{pv} , W_{pv} , and K are the height, width, and feature dimension respectively.

Neural view transformer. As shown in Figure 3, we first transform image features from perspective view to camera coordinate system and then to bird’s-eye view. The relation of any two pixels between perspective view and camera coordinate system is modeled by a multi-layer perceptron $\phi_{\mathcal{V}_i}$:

$$\mathcal{F}_{\mathcal{I}_i}^c[h][w] = \phi_{\mathcal{V}_i}^{hw}(\mathcal{F}_{\mathcal{I}_i}^{\text{pv}}[1][1], \dots, \mathcal{F}_{\mathcal{I}_i}^{\text{pv}}[H_{\text{pv}}][W_{\text{pv}}]) \quad (1)$$

where $\phi_{\mathcal{V}_i}^{hw}$ models the relation between feature vector at position (h, w) in the camera coordinate system and every pixel on the perspective view feature map. We denote H_c and W_c as the top-down spatial dimensions of $\mathcal{F}_{\mathcal{I}_i}^c$. The bird’s-eye view (ego coordinate system) features $\mathcal{F}_{\mathcal{I}_i}^{\text{bev}} \subseteq \mathbb{R}^{H_{\text{bev}} \times W_{\text{bev}} \times K}$ is obtained by transforming the features $\mathcal{F}_{\mathcal{I}_i}^c$ using geometric projection with camera extrinsics, where H_{bev} and W_{bev} are the height and width in the bird’s-eye view. The final image feature $\mathcal{F}_{\mathcal{I}}^{\text{bev}}$ is an average of N_m camera features.

3.1.2 Point cloud encoder

Our point cloud encoder ϕ_P is a variant of PointPillar [39] with dynamic voxelization [40], which divide the 3d space into multiple pillars and learn feature maps from pillar-wise features of pillar-wise point clouds. The input is N lidar points in the point cloud. For each point p , it has three-dimensional coordinates and additional K -dimensional features represented as $f_p \subseteq \mathbb{R}^{K+3}$.

When projecting features from points to bird’s-eye view, multiple points can potentially fall into the same pillar. We define P_j as the set of points corresponding to pillar j . To aggregate features from points in a pillar, a PointNet [41] (denoted as PN) is warranted, where

$$f_j^{\text{pillar}} = \text{PN}(\{f_p | \forall p \in P_j\}). \quad (2)$$

Then, pillar-wise features are further encoded through a convolutional neural network ϕ_{pillar} . We denote the feature map in the bird’s-eye view as $\mathcal{F}_P^{\text{bev}}$.

3.1.3 Bird’s-eye view decoder

The map is a complex graph network that includes instance-level and directional information of lane dividers and lane boundaries. Instead of pixel-level representation, lane lines need to be vectorized so that they can be followed by self-driving vehicles. Therefore, our BEV decoder $\phi_{\mathcal{M}}$ not only outputs semantic segmentation but also predicts instance embedding and lane direction. A post-processing process is applied to cluster instances from embeddings and vectorize them.

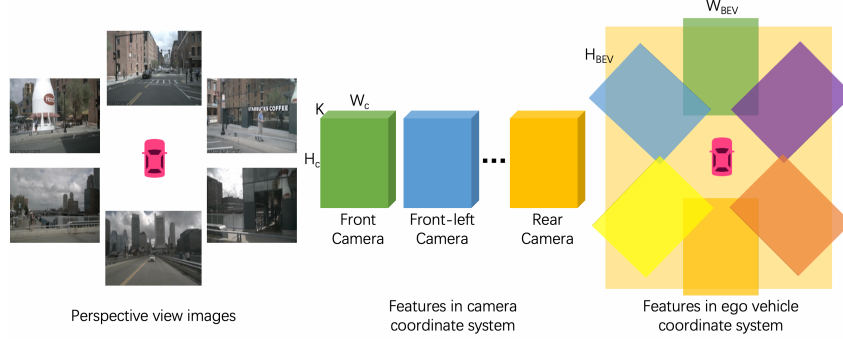


Figure 3: Feature transformation. Left: the 6 input images in the perspective view. Middle: 6 feature maps in camera coordinate system, which are obtained by extracting features using image encoder and transforming these features with MLP; each feature map (in different colors) covers a certain area. Right: the feature map (in orange) in the ego vehicle coordinate system; this is fused from 6 feature maps and transformed to the ego vehicle coordinate system with camera extrinsics.

Overall architecture. The BEV decoder is a fully convolutional network (FCN) [42] with 3 branches, namely semantic segmentation branch, instance embedding branch, and direction prediction branch. The input of BEV decoder is image feature map F_T^{bev} and/or point cloud feature map F_P^{bev} , and we concatenate them if both exist.

Instance embedding. Our instance embedding module seeks to cluster each bird’s-eye view embedding. For ease of notation, we follow the exact definition in [43]: C is the number of clusters in the ground truth, N_c is the number of elements in cluster c , μ_c is the mean embedding of cluster c , $\|\cdot\|$ is the L1 norm, and $[x]_+ = \max(0, x)$ denotes the element maximum. δ_v and δ_d are respectively the margins for the variance and distance loss. The clustering loss L is computed by:

$$L_{var} = \frac{1}{C} \sum_{c=1}^C \frac{1}{N_c} \sum_{j=1}^{N_c} [\|\mu_c - f_j^{\text{instance}}\| - \delta_v]_+^2 \quad (3)$$

$$L_{dist} = \frac{1}{C(C-1)} \sum_{c_A \neq c_B \in C} [2\delta_d - \|\mu_{c_A} - \mu_{c_B}\|]_+^2, \quad (4)$$

$$L = \alpha L_{var} + \beta L_{dist}. \quad (5)$$

Direction prediction. Our direction module aims to classify directions of lanes from each lane node C on a unit circle having N_d discrete directions. By predicated direction D of current node C_{now} , the next node of lane C_{next} can be obtained as follows:

$$C_{next} = C_{now} + \Delta_{step} \cdot D \quad (6)$$

where Δ_{step} is a predefined step size. Since we don’t know the direction of the lane, we cannot identify the forward and backward direction of each node. Instead, we treat both of them as positive labels. Concretely, the direction label of each lane node is a N_d vector with 2 indices labeled as 1 and others labeled as 0. Note that most of the pixels on the topdown map don’t lie on the lanes, which means they don’t have directions. The direction vector of those pixels is a zero vector and we never do backpropagation for those pixels during training. We use softmax as the activation function for classification.

Vectorization. During inference, we first cluster instance embeddings using the Density-Based Spatial Clustering of Applications with Noise (DBSCAN). Then non-maximum suppression (NMS) is used to reduce redundancy. Finally, the vector representations are obtained by greedily connecting the pixels with the help of the predicted direction. Please see appendix for pseudocode.

3.2 Evaluation

In this section, we propose evaluation protocols for online map learning, including semantic metrics and instance metrics.

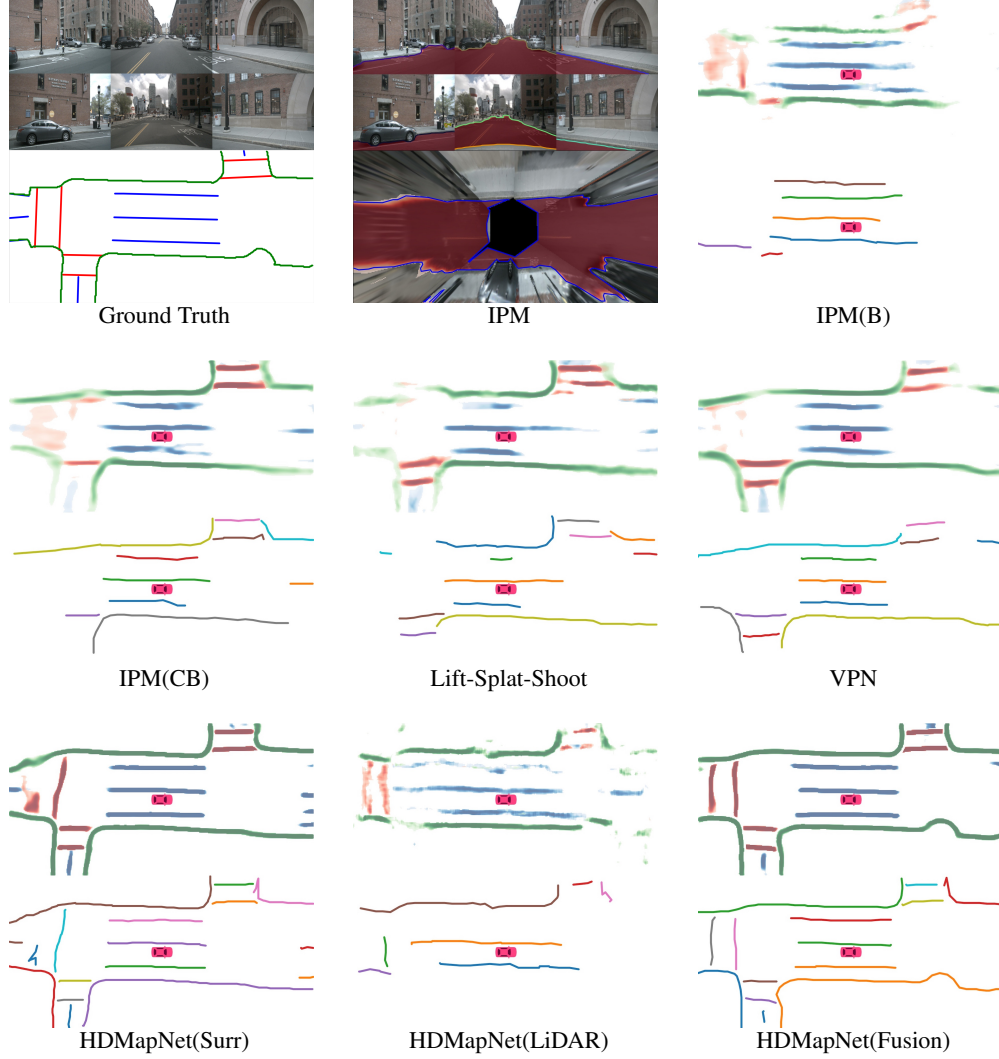


Figure 4: Qualitative results on the validation set. Top left: we show the surrounding images and the ground-truth local HD Map annotations. IPM: we show the lane segmentation result in the perspective view and the bird’s-eye view. Others: we show the semantic segmentation results and the vectorized instance detection results.

3.2.1 Semantic metrics

The semantics of model predictions can be evaluated in the *Eulerian* fashion and the *Lagrangian* fashion. *Eulerian* metrics are computed on a dense grid and measure the pixel value differences. In contrast, *Lagrangian* metrics move with the shape and measure the spatial distances of shapes.

Eulerian metrics. We use intersection-over-union (IoU) as Eulerian metrics, which is given by,

$$\text{IoU}(\mathcal{D}_1, \mathcal{D}_2) = \frac{|\mathcal{D}_1 \cap \mathcal{D}_2|}{|\mathcal{D}_1 \cup \mathcal{D}_2|}, \quad (7)$$

where $\mathcal{D}_1, \mathcal{D}_2 \subseteq \mathbb{R}^{H \times W \times D}$ are dense representations of shapes (curves rasterized on a grid); H and W are the height and width of the grid while D is number of categories; $|\cdot|$ denotes the size of the set.

Lagrangian metrics. We are interested in structured outputs, namely curves consists of connected points. To evaluate the spatial distances between the predicted curves and ground-truth curves, we

Table 1: IoU scores (%) and CD (m) of semantic map segmentation. CD_P denotes the CD from label to prediction (equivalent to precision) while CD_L denotes the CD from Prediction to Label (equivalent to recall); CD is the average of them. IoU: higher is better. CD: lower is better. *: the perspective view labels projected from 2D HD Maps.

Method	Divider				Ped Crossing				Boundary				All Classes			
	IoU	CD_P	CD_L	CD	IoU	CD_P	CD_L	CD	IoU	CD_P	CD_L	CD	IoU	CD_P	CD_L	CD
IPM*	14.4	1.149	2.232	2.193	9.5	1.232	3.432	2.482	18.4	1.502	2.569	1.849	14.1	1.294	2.744	2.175
IPM(B)	25.5	1.091	1.730	1.226	12.1	0.918	2.947	1.628	27.1	0.710	1.670	0.918	21.6	0.906	2.116	1.257
IPM(CB)	38.6	0.743	1.106	0.802	19.3	0.741	2.154	1.081	39.3	0.563	1.000	0.633	32.4	0.682	1.42	0.839
Lift-Splat-Shoot [38]	38.3	0.872	1.144	0.916	14.9	0.680	2.691	1.313	39.3	0.580	1.137	0.676	30.8	0.711	1.657	0.968
VPN [36]	36.5	0.534	1.197	0.919	15.8	0.491	2.824	2.245	35.6	0.283	1.234	0.848	29.3	0.436	1.752	1.337
HDMNet(Surr)	40.6	0.761	0.979	0.779	18.7	0.855	1.997	1.101	39.5	0.608	0.825	0.624	32.9	0.741	1.267	0.834
HDMNet(LiDAR)	26.7	1.134	1.508	1.219	17.3	1.038	2.573	1.524	44.6	0.501	0.843	0.561	29.5	0.891	1.641	1.101
HDMNet(Fusion)	46.1	0.625	0.893	0.667	31.4	0.535	1.715	0.790	56.0	0.461	0.443	0.459	44.5	0.540	1.017	0.639

use Chamfer distance (CD) of between point sets sampled on the curves:

$$CD_{Dir}(\mathcal{S}_1, \mathcal{S}_2) = \frac{1}{|\mathcal{S}_1|} \sum_{x \in \mathcal{S}_1} \min_{y \in \mathcal{S}_2} \|x - y\|_2 \quad CD(\mathcal{S}_1, \mathcal{S}_2) = CD_{Dir}(\mathcal{S}_1, \mathcal{S}_2) + CD_{Dir}(\mathcal{S}_2, \mathcal{S}_1) \quad (8)$$

where CD_{dir} is the directional Chamfer distance and CD is the bi-directional Chamfer distance; \mathcal{S}_1 and \mathcal{S}_2 are the two sets of points on the curves.

3.2.2 Instance metrics

We further evaluate the instance detection capability of our models. We use average precision (AP) similar to the one in object detection [44], given by

$$AP = \frac{1}{10} \sum_{r \in \{0.1, 0.2, \dots, 1.0\}} AP_r, \quad (9)$$

where AP_r is the precision at recall= r . To do so, we collect all predictions and rank them in descending order according to the semantic confidences. Then, we classify each prediction based on the CD threshold. For example, if the CD is lower than a predefined threshold, it is considered true positive, otherwise false positive. Finally, we obtain all precision-recall pairs and compute APs accordingly.

4 Experiments

4.1 Implementation details

Tasks & Metrics. We evaluate our approach on the NuScenes dataset [45]. In this paper, we mainly focus on two tasks: HD Map semantic segmentation and instance detection. Due to the limited types of map elements in the nuScenes dataset, we consider three static map elements: lane boundary, lane divider, and pedestrian crossing. To evaluate semantic segmentation, we use both IoU (Equation 7) and CD (Equation 8). For HD Map instance detection, We compute AP (Equation 9) as in COCO [44] at threshold $CD=0.2m, 0.5m$, and $1.0m$.

Architecture. For the perspective view image encoder, we adopt EfficientNet-B0 [46] pre-trained on ImageNet [47], as in [38]. Then, we use a multi-layer perceptron (MLP) to convert the perspective view features to bird’s-eye view features in the camera coordinate system. The MLP is shared channel-wisely and does not change the feature dimension. For point clouds, we use a variant of PointPillars [48] with dynamic voxelization [40]. We use a PointNet [41] with a 64-dimensional layer to aggregate points in a pillar. ResNet [49] with three blocks is used as the BEV decoder. The final feature map is upsampled to the same size as the prediction target.

Training details. We use the cross-entropy loss for the semantic segmentation use the discriminative loss (Equation 5) for the instance embedding where we set $\alpha = \beta = 1$, $\delta_v = 0.5$, and $\delta_d = 3.0$. We use Adam [50] for model training, with a learning rate of $1e - 3$.

4.2 Baseline methods

Inverse Perspective Mapping (IPM). The most straightforward baseline to construct an HD Map is to map semantic segmentation predictions to the bird’s-eye view via IPM [51, 52]. Although IPM

works well for local road layout, it has two major drawbacks: IPM assumes a flat ground plane, which is not realistic in many scenarios; predictions in each perspective view image are not easily ensembled to a continuous and holistic view. We use FPN [53] with resnext50_32x4d [54] backbone to segment each image. Then, we project the predictions via IPM to bird’s-eye view. In this paper, we assume the ground plane is $z = 0$ in the vehicle coordinate system and use intrinsic and extrinsic in nuScenes dataset to perform homographic projection.

IPM with bird’s-eye view decoder (IPM(B)). Our second baseline is an extension of IPM. Rather than making predictions in perspective view, we perform semantic segmentation directly in bird-eye view. We use the same decoder network as in HDMaNet.

IPM with perspective view feature encoder and bird’s-eye view decoder (IPM(CB)). The next extension is to perform feature learning in the perspective view while making predictions in the bird’s-eye view. We use the same image encoder and BEV decoder as in HDMaNet.

Lift-Splat-Shoot. Lift-Splat-Shoot [38] estimates a distribution over depth in the perspective view images. Then, it converts 2D images into 3D point clouds with features and projects them into the ego vehicle frame. Finally, the point clouds are transformed to a bird’s-eye view feature map with PointPillars [48]. We use the code provided by [38] for experiments.

View Parsing Network (VPN). VPN proposes a simple view transformation module to transform feature map from the perspective view to bird’s-eye view: it uses a view relation module (VRM) (a two-layer MLPs) to model the relations between any two pixels in the perspective view feature map; then, a view fusion module (VFM) with average pooling layer fuse the features of pixels that fall into the same bird’s-eye view position. We use the code released by [36] for experiments.

4.3 Results

Semantic map segmentation. We compare our HDMaNet against baselines in §4.2. Table 1 shows the comparisons. First, Our HDMaNet(Surr), which is the surrounding camera-only method, outperforms all baselines. This suggests that our novel learning-based view transformation is indeed effective, without making impractical assumptions about a complex ground plane (IPM) or estimating the depth (Lift-Splat-Shoot). Second, our HDMaNet(LiDAR) is better than HDMaNet(Surr) in boundary but worse in divider and pedestrian crossing. This indicates different categories are not equally recognizable in one modality. Third, our fusion model with both camera images and LiDAR point clouds achieves the best performance. It improves over baselines and our camera-only method by 50% relatively.

Another interesting phenomenon is that various models behave differently in terms of the CD. For example, VPN has the lowest CD_P in all categories, while it underperforms its counterparts on CD_L and has the worst overall CD. Instead, our HDMaNet(Surr) balances both CD_P and CD_L , achieving the best CD among all camera-only-based methods. This finding indicates that CD is complementary to IoU, which shows the precision and recall aspects of models. This helps us understand the behaviors of different models from another perspective.

Instance map detection. In Figure 2 (Instance detection branch), we show the visualization of embeddings using principal component analysis (PCA). Different lanes are assigned different colors even when they are close to each other or have intersections. This confirms our model learns instance-level information and can predict instance labels accurately. In Figure 2 (Direction classification branch), we show the direction mask predicted by our direction branch. The direction is consistent and smooth. We show the vectorized curve produced after post processing in Figure 4. In Table 2, we present the quantitative results of instance map detection. HDMaNet(Surr) already outperforms baselines while HDMaNet(Fusion) is significantly better than all counterparts, e.g., it improves over IPM by 55.4%.

Sensor fusion. In this section, we further analyze the effect of sensor fusion for constructing local HD Maps. As shown in Table 1, for divider and pedestrian crossing, HDMaNet(Surr) outperforms HDMaNet(LiDAR), while for lane boundary, HDMaNet(LiDAR) works better. We hypothesize this is because there are elevation changes near the land boundary, making it easy to detect in LiDAR point clouds. On the other hand, the color contrast of road divider and pedestrian crossing is helpful information, making two categories more recognizable in images; visualizations also confirm this in Figure 4. The strongest performance is achieved when combining LiDAR and cameras; the

Table 2: Instance detection results. $\{0.2, 0.5, 1.\}$ are the predefined thresholds of Chamfer distance (*e.g.* a prediction is considered a true positive if the Chamfer distance between label and prediction is lower than that threshold). The mAP is the average of three APs. AP & mAP: higher is better.

Method	Divider				Ped Crossing				Boundary				All Classes			
	AP@.2	AP@.5	AP@1.	mAP	AP@.2	AP@.5	AP@1.	mAP	AP@.2	AP@.5	AP@1.	mAP	AP@.2	AP@.5	AP@1.	mAP
IPM(B)	2.6	9.8	19.6	10.7	1.6	4.8	7.8	4.7	2.2	9.2	23.7	11.7	2.1	7.9	17.0	9.0
IPM(CB)	10.2	25.0	36.8	24.0	2.0	7.8	12.2	7.3	10.1	27.9	45.5	27.8	7.4	20.2	31.5	19.7
Lift-Splat-Shoot [38]	9.1	23.8	35.9	22.9	0.9	5.4	8.9	5.1	8.5	22.9	41.2	24.2	6.2	17.4	28.7	17.4
VPN [36]	8.8	22.7	34.9	22.1	1.2	5.3	9.0	5.2	9.2	24.1	42.7	25.3	6.4	17.4	28.9	17.5
HDMaNet(Surr)	13.7	30.7	40.6	28.3	1.9	7.4	12.1	7.1	13.7	33.9	50.1	32.6	9.8	24.0	34.3	22.7
HDMaNet(LiDAR)	1.0	5.7	15.1	7.3	1.9	5.8	9.0	5.6	5.8	20.2	39.6	21.9	2.9	10.6	21.2	11.6
HDMaNet(Fusion)	15.0	32.6	46.0	31.2	6.4	13.6	17.8	12.6	26.7	51.5	65.6	47.9	16.0	32.6	43.1	30.6

combined model outperforms both models with a single sensor by a large margin. This suggests these two sensors include complementary information for each other.

5 Conclusion

HDMaNet tackles the online map learning problem. The success of HDMaNet verifies that we can predict the map directly from camera images and/or LiDAR point clouds. This could be a more scalable approach than the traditional pipeline that requires a significant amount of human effort. We hope our method provides insights into design choices of the perception and the mapping in autonomous driving and robotics broadly.

Beyond its direct usage, our experiments suggest several avenues for future inquiry. First, camera images and LiDAR point clouds complement each other; adding more modalities and searching for better fusion strategies can potentially improve the generalizability and stability of the self-driving system. Another possible extension is to add temporal information to HDMaNet since planning algorithms require temporally coherent maps. Finally, using the online maps for downstream tasks such as behavior prediction, motion planning remains an interesting and open problem.

References

- [1] M. Elhousni and X. Huang. A survey on 3d lidar localization for autonomous vehicles. In *2020 IEEE Intelligent Vehicles Symposium (IV)*, pages 1879–1884. IEEE.
- [2] S. Bauer, Y. Alkhorshid, and G. Wanielik. Using high-definition maps for precise urban vehicle localization. In *2016 IEEE 19th International Conference on Intelligent Transportation Systems (ITSC)*, pages 492–497. IEEE, 2016.
- [3] S. Thrun. Simultaneous localization and mapping. In *Robotics and cognitive approaches to spatial mapping*, pages 13–41. Springer, 2007.
- [4] J. Gao, C. Sun, H. Zhao, Y. Shen, D. Anguelov, C. Li, and C. Schmid. Vectornet: Encoding hd maps and agent dynamics from vectorized representation. In *Proceedings of the IEEE/CVF Conference on Computer Vision and Pattern Recognition*, pages 11525–11533, 2020.
- [5] H. Zhao, J. Gao, T. Lan, C. Sun, B. Sapp, B. Varadarajan, Y. Shen, Y. Shen, Y. Chai, C. Schmid, et al. Tnt: Target-driven trajectory prediction. *arXiv preprint arXiv:2008.08294*, 2020.
- [6] A. Chen, A. Ramanandan, and J. A. Farrell. High-precision lane-level road map building for vehicle navigation. In *IEEE/ION position, location and navigation symposium*, pages 1035–1042. IEEE, 2010.
- [7] S. M. LaValle. Rapidly-exploring random trees: A new tool for path planning. 1998.
- [8] G. Grisetti, R. Kümmerle, C. Stachniss, and W. Burgard. A tutorial on graph-based slam. *IEEE Intelligent Transportation Systems Magazine*, 2(4):31–43, 2010.
- [9] S. Thrun. Probabilistic robotics. *Communications of the ACM*, 45(3):52–57, 2002.
- [10] S. Yang, X. Zhu, X. Nian, L. Feng, X. Qu, and T. Ma. A robust pose graph approach for city scale lidar mapping. In *2018 IEEE/RSJ International Conference on Intelligent Robots and Systems (IROS)*, pages 1175–1182. IEEE, 2018.

- [11] J. Jiao. Machine learning assisted high-definition map creation. In *2018 IEEE 42nd Annual Computer Software and Applications Conference (COMPSAC)*, volume 1, pages 367–373. IEEE, 2018.
- [12] P. Egger, P. V. Borges, G. Catt, A. Pfrunder, R. Siegwart, and R. Dubé. Posemap: Lifelong, multi-environment 3d lidar localization. In *2018 IEEE/RSJ International Conference on Intelligent Robots and Systems (IROS)*, pages 3430–3437. IEEE, 2018.
- [13] P. J. Besl and N. D. McKay. Method for registration of 3-d shapes. In *Sensor fusion IV: control paradigms and data structures*, volume 1611, pages 586–606. International Society for Optics and Photonics, 1992.
- [14] P. Biber and W. Straßer. The normal distributions transform: A new approach to laser scan matching. In *Proceedings 2003 IEEE/RSJ International Conference on Intelligent Robots and Systems (IROS 2003)(Cat. No. 03CH37453)*, volume 3, pages 2743–2748. IEEE, 2003.
- [15] A. Segal, D. Haehnel, and S. Thrun. Generalized-icp. In *Robotics: science and systems*, volume 2, page 435. Seattle, WA, 2009.
- [16] F. Yu, J. Xiao, and T. Funkhouser. Semantic alignment of lidar data at city scale. In *Proceedings of the IEEE Conference on Computer Vision and Pattern Recognition*, pages 1722–1731, 2015.
- [17] F. Pomerleau, F. Colas, and R. Siegwart. A review of point cloud registration algorithms for mobile robotics. *Foundations and Trends in Robotics*, 4(1):1–104, 2015.
- [18] C. L. Lawson and R. J. Hanson. *Solving least squares problems*. SIAM, 1995.
- [19] F. Dellaert. Factor graphs and gtsam: A hands-on introduction. Technical report, Georgia Institute of Technology, 2012.
- [20] K.-Y. Chiu and S.-F. Lin. Lane detection using color-based segmentation. In *IEEE Proceedings. Intelligent Vehicles Symposium, 2005.*, pages 706–711. IEEE, 2005.
- [21] H. Loose, U. Franke, and C. Stiller. Kalman particle filter for lane recognition on rural roads. In *2009 IEEE Intelligent Vehicles Symposium*, pages 60–65. IEEE, 2009.
- [22] S. Zhou, Y. Jiang, J. Xi, J. Gong, G. Xiong, and H. Chen. A novel lane detection based on geometrical model and gabor filter. In *2010 IEEE Intelligent Vehicles Symposium*, pages 59–64. IEEE, 2010.
- [23] J. Illingworth and J. Kittler. A survey of the hough transform. *Computer vision, graphics, and image processing*, 44(1):87–116, 1988.
- [24] J. M. Alvarez, T. Gevers, Y. LeCun, and A. M. Lopez. Road scene segmentation from a single image. In *ECCV*, 2012.
- [25] B. Zhou, H. Zhao, X. Puig, S. Fidler, A. Barriuso, and A. Torralba. Scene parsing through ade20k dataset. In *Proceedings of the IEEE conference on computer vision and pattern recognition*, pages 633–641, 2017.
- [26] A. Ess, T. Mueller, H. Grabner, and L. Van Gool. Segmentation-based urban traffic scene understanding. In *BMVC*, volume 1, page 2. Citeseer, 2009.
- [27] M. Cordts, M. Omran, S. Ramos, T. Rehfeld, M. Enzweiler, R. Benenson, U. Franke, S. Roth, and B. Schiele. The cityscapes dataset for semantic urban scene understanding. In *CVPR*, 2016.
- [28] F. Yu, W. Xian, Y. Chen, F. Liu, M. Liao, V. Madhavan, and T. Darrell. Bdd100k: A diverse driving video database with scalable annotation tooling. *arXiv preprint arXiv:1805.04687*, 2(5):6, 2018.
- [29] G. Neuhold, T. Ollmann, S. Rota Bulò, and P. Kotschieder. The mapillary vistas dataset for semantic understanding of street scenes. In *Proceedings of the IEEE International Conference on Computer Vision*, pages 4990–4999, 2017.

- [30] Z. Wang, W. Ren, and Q. Qiu. Lanenet: Real-time lane detection networks for autonomous driving. *arXiv preprint arXiv:1807.01726*, 2018.
- [31] D. Neven, B. De Brabandere, S. Georgoulis, M. Proesmans, and L. Van Gool. Towards end-to-end lane detection: an instance segmentation approach. In *2018 IEEE intelligent vehicles symposium (IV)*, pages 286–291. IEEE, 2018.
- [32] X. Liu and Z. Deng. Segmentation of drivable road using deep fully convolutional residual network with pyramid pooling. *Cognitive Computation*, 10(2):272–281, 2018.
- [33] M. Bai, G. Mattyus, N. Homayounfar, S. Wang, K. Lakshmikanth, Shrinidhi, and R. Urtasun. Deep multi-sensor lane detection. In *IROS*, 2018.
- [34] N. Garnett, R. Cohen, T. Pe’er, R. Lahav, and D. Levi. 3d-lanenet: end-to-end 3d multiple lane detection. In *Proceedings of the IEEE/CVF International Conference on Computer Vision*, pages 2921–2930, 2019.
- [35] Y. Guo, G. Chen, P. Zhao, W. Zhang, J. Miao, J. Wang, and T. E. Choe. Genlanenet: A generalized and scalable approach for 3d lane detection. 2020.
- [36] B. Pan, J. Sun, H. Y. T. Leung, A. Andonian, and B. Zhou. Cross-view semantic segmentation for sensing surroundings. *IEEE Robotics and Automation Letters*, 5(3):4867–4873, Jul 2020. ISSN 2377-3774. doi:10.1109/lra.2020.3004325. URL <http://dx.doi.org/10.1109/LRA.2020.3004325>.
- [37] T. Roddick and R. Cipolla. Predicting semantic map representations from images using pyramid occupancy networks. In *Proceedings of the IEEE/CVF Conference on Computer Vision and Pattern Recognition*, pages 11138–11147, 2020.
- [38] J. Philion and S. Fidler. Lift, splat, shoot: Encoding images from arbitrary camera rigs by implicitly unprojecting to 3d, 2020.
- [39] A. H. Lang, S. Vora, H. Caesar, L. Zhou, J. Yang, and O. Beijbom. Pointpillars: Fast encoders for object detection from point clouds. In *The IEEE Conference on Computer Vision and Pattern Recognition (CVPR)*, June 2019.
- [40] Y. Zhou, P. Sun, Y. Zhang, D. Anguelov, J. Gao, T. Ouyang, J. Guo, J. Ngiam, and V. Vasudevan. End-to-end multi-view fusion for 3d object detection in LiDAR point clouds. In *The Conference on Robot Learning (CoRL)*, 2019.
- [41] C. R. Qi, H. Su, K. Mo, and L. J. Guibas. Pointnet: Deep learning on point sets for 3d classification and segmentation. In *The IEEE Conference on Computer Vision and Pattern Recognition (CVPR)*, July 2017.
- [42] E. Shelhamer, J. Long, and T. Darrell. Fully convolutional networks for semantic segmentation. *IEEE Transactions on Pattern Analysis and Machine Intelligence*, 39(4):640–651, 2017.
- [43] B. De Brabandere, D. Neven, and L. Van Gool. Semantic instance segmentation for autonomous driving. In *Proceedings of the IEEE Conference on Computer Vision and Pattern Recognition (CVPR) Workshops*, July 2017.
- [44] T.-Y. Lin, M. Maire, S. Belongie, L. Bourdev, R. Girshick, J. Hays, P. Perona, D. Ramanan, C. L. Zitnick, and P. Dollár. Microsoft coco: Common objects in context, 2015.
- [45] H. Caesar, V. Bankiti, A. H. Lang, S. Vora, V. E. Liong, Q. Xu, A. Krishnan, Y. Pan, G. Baldan, and O. Beijbom. nuscenes: A multimodal dataset for autonomous driving, 2020.
- [46] M. Tan and Q. V. Le. Efficientnet: Rethinking model scaling for convolutional neural networks, 2020.
- [47] O. Russakovsky, J. Deng, H. Su, J. Krause, S. Satheesh, S. Ma, Z. Huang, A. Karpathy, A. Khosla, M. Bernstein, A. C. Berg, and L. Fei-Fei. Imagenet large scale visual recognition challenge, 2015.

- [48] A. H. Lang, S. Vora, H. Caesar, L. Zhou, J. Yang, and O. Beijbom. Pointpillars: Fast encoders for object detection from point clouds, 2019.
- [49] K. He, X. Zhang, S. Ren, and J. Sun. Deep residual learning for image recognition. In *CVPR*, 2016.
- [50] D. P. Kingma and J. Ba. Adam: A method for stochastic optimization, 2017.
- [51] L. Deng, M. Yang, H. Li, T. Li, B. Hu, and C. Wang. Restricted deformable convolution-based road scene semantic segmentation using surround view cameras. *IEEE Transactions on Intelligent Transportation Systems*, 21(10):4350–4362, Oct 2020. ISSN 1558-0016. doi:10.1109/tits.2019.2939832. URL <http://dx.doi.org/10.1109/TITS.2019.2939832>.
- [52] T. S  mann, K. Amende, S. Milz, C. Witt, M. Simon, and J. Petzold. Efficient semantic segmentation for visual bird’s-eye view interpretation, 2018.
- [53] T.-Y. Lin, P. Doll  r, R. Girshick, K. He, B. Hariharan, and S. Belongie. Feature pyramid networks for object detection, 2017.
- [54] S. Xie, R. Girshick, P. Doll  r, Z. Tu, and K. He. Aggregated residual transformations for deep neural networks, 2017.

A Post-processing methods

Algorithm 1: Vectorization(S, C, D)

Data: segmentation S , cluster embedding C , direction D

Result: Vectorized HD Map

lines_cloud = DBSCAN(S, C);

vectorized_lines = [];

foreach line_cloud in lines_cloud **do**

 sparse_line = Directional_NMS(line_cloud);

 vector_line = Connect_Line(sparse_line, D);

 vectorized_lines.append(vector_line);

end

return vectorized_lines

Algorithm 2: Directional_NMS(L)

Data: line point cloud L with confidence

Result: sparse line point cloud L'

mp_vertical = MaxPool2d(1, 5);

mp_horizontal = MaxPool2d(5, 1);

ap_vertical = AvgPool2d(5, 9);

ap_horizontal = AvgPool2d(9, 5);

$L' = L$;

foreach $p \in L$ **do**

if ap_vertical(p) > ap_horizontal(p) **then**

if mp_horizontal(p) != p **then**

 drop p from L' ;

end

else

if mp_vertical(p) != p **then**

 drop p from L' ;

end

end

end

return L'

Algorithm 3: Connect_Line(L , D)

Data: line point cloud L , direction D

Result: vector line L'

```
p = random_sample(L);  
line_1 = Connect_One_Direction(p, L, D);  
line_2 = Connect_One_Direction(p, L, D);  
vector_line = concat(line_1, reverse(line_2));  
return vector_line
```

Algorithm 4: Connect_One_Direction(p , L , D)

Data: start point p , line point cloud L , direction D

Result: one direction connected vector line L'

```
while  $L$  is not empty do  
  if Direction  $pd$  of  $p$  is not taken then  
    | pick  $pd$  and mark it as taken;  
  else  
    | break;  
  end  
   $p_{target} = p + pd * step$ ;  
  remove  $p'$  in  $L$  where  $dist(p, p') < step-1$ ;  
   $p_{next} = \min(dist(p', p_{target}))$  where  $p'$  in  $L$ ;  
  if  $dist(p, p_{next}) > threshold$  then  
    | break  
  end  
  vector_line.append( $p_{next}$ );  
  mark the connected direction of  $p_{next}$  as taken;  
   $p = p_{next}$ ;  
end  
return vector_line
```
